Landscape Online – transdisciplinary journal bridging science, policy and practice
Supported by the International Association for Landscape Ecology and its community

Landscape Online
open access peer reviewed

RESEARCH ARTICLE

Landscape Online | Volume 99 | 2024 | Article 1130

Submitted: 26 January 2024 | Accepted in revised version: 19 December 2024| Published: 31 December 2024

# Assessing Short-term Flood Impact on Land Use Dynamics in Iran's Central Zagros: A Case Study of Sefid Kuh Protected Area

## Abstract

Floods are extreme events that can alter the land cover and land use patterns in mountainous regions, with significant consequences for biodiversity, ecosystem services, and human well-being. However, there is a lack of comprehensive and integrated studies on the short-term and long-term effects of floods on land cover dynamics in the Central Zagros region, which is a climate change hotspot and a protected area with rich flora and fauna. In this study, we aimed to assess the effects of floods on land cover changes and transitions in the Sefid Kuh Protected Area, Lorestan Province in Iran, using temporal satellite imagery from Landsat 8, land-use/land-cover change detection and fragmentation analysis, and landscape pattern indices. We also conducted fieldwork and interviews to evaluate the impact of floods on land cover from the ground and from the local people's perspectives. Our results showed that floods caused significant disturbances and shifts in different land cover classes, such as Thin Woodlands, Thick Woodlands, Agriculture, Rock, and Snow. For the landscape pattern indices the Shannon's Diversity Index (SHDI), Interspersion and Juxtaposition Index (IJI), Patch Density (PD), Edge Density (ED), Largest Patch Index (LPI), Aggregation Index (AI), Percentage of Land Area (PLAND), Number of Patches (NP), Total Edge (TE), Landscape Shape Index (LSI), and Splitting Index (SPLIT) have been used. Results revealed that floods reduced the diversity and heterogeneity of the landscape, increased the fragmentation and isolation of forest patches, and enhanced the aggregation and clumpiness of bare soil patches. These changes have implications for the resilience and adaptation of the study area to future flood hazards and climate change.

**Soheyl Moradi[1], Hossein Moradi[2,3], Jafar Dolatshah[4], Azita Rezvani[3*]**

1) Institute of Geography, Slovak Academy of Sciences, Bratislava, Slovakia

2) Department of Environmental Science and Engineering, Faculty of Natural Resources, University College of Agriculture and Natural Resources, University of Tehran, Karaj, Iran

3) Department of Natural Resources, Isfahan University of Technology, Isfahan, Iran

4) Department of Environmental (DoE) of Lorestan Province, Lorestan, Iran

*Corresponding author email: azita.rezvani@na.iut.ac.ir

Soheyl Moradi
https://orcid.org/0009-0003-8372-6957

Hossein Moradi
https://orcid.org/ 0009-0001-5885-9569

Azita Rezvani
https://orcid.org/0000-0002-7808-246X

**Keywords:**
land-use/land-cover change detection, fragmentation analysis, flood interference, Central Zagros, Sefid kuh protected area, Landsat 8; landscape pattern indices

https://doi.org/10.3097/LO.2024.1130

© 2024 The Authors. Published in Landscape Online – www.Landscape-Online.org

Open Access Article distributed under the terms of the Creative Commons Attribution 4.0 International License (CC BY 4.0), which permits unrestricted use, distribution, and reproduction in any medium, provided the original work is properly cited.

## 1 Introduction

Floods are extreme events that surpass the usual range of natural variability due to climate change. These events are exceptional in their intensity, duration, or frequency, leading to abrupt and profound environmental changes over short periods. Floods can have significant consequences for land use and land cover dynamics, often challenging the resilience of ecosystems that are adapted to regular disturbance regimes (Schaller et al., 2016). Floods, as a natural component of river systems, play a crucial role in maintaining the ecological integrity of floodplain habitats. They contribute to nutrient cycling, groundwater recharge, and the creation of diverse habitat mosaics (Whited et al., 2007). However, severe floods can also cause extensive damage to human infrastructure, agriculture, and natural resources, posing significant challenges for land management and urban planning (Ward et al., 2020). It is projected that global financial losses due to floods will increase from 6 billion dollars in 2005 to 52 billion dollars by 2050 (Hallegatte 2016). Floods result in damage to natural resources, loss of human life, and global economic damage, and these effects are to some extent inevitable and natural (Jönsson et al., 2015). Several factors contribute to land use deterioration and disruption to watershed hydrological functions. These factors include deviations from local or regional spatial plans, which are comprehensive frameworks designed to guide land use and development within specific areas. Regional spatial plans encompass broader geographic regions and aim to coordinate land use policies across multiple municipalities to ensure sustainable development and environmental protection. Other contributing factors include discrepancies between land use in the watershed and land capacity, violations of soil management standards in land treatment within the watershed, and the absence of land and water management strategies that mandate appropriate soil and water conservation practices in agricultural land use (Chalid, 2020; Stolpe et al., 2022). Vegetation mitigates the impact of floods by scattering Stream Energy, and stabilizing margins, sides, and slopes against erosion (Croke et al., 2017). It enhances soil cohesion and infiltration, reducing runoff and flash floods. Plant roots anchor the soil, preventing erosion, while vegetative cover slows water flow, promoting sediment deposition and reducing kinetic energy (Anderson et al., 2006). Vegetation also boosts biodiversity and ecosystem health, increasing resilience to disturbances. Effective riparian vegetation management is essential for maintaining riverbank and coastal integrity, offering a natural, sustainable approach to flood mitigation (Crossman et al., 2019; Bolan et al., 2023; Birkeland et al., 1979). In a study by Verbesselt et al. (2010), a general approach to land use detection was proposed, utilizing seasonal change detection, and analyzing various trends such as deforestation, urbanization, and seasonal floods through time series of the NDVI index. This method has proven effective in monitoring and detecting land cover changes over time. Subsequent research has expanded on this approach, incorporating additional techniques and datasets. For instance, Lin et al. (2020) demonstrated the use of NDVI time series for separating different types of land cover changes, enhancing the precision of detection algorithms.

Additionally, Zhu (2022) noted a paradigm shift from traditional two-point change detection to continuous monitoring, which has enhanced the ability to track and analyze land cover changes over time (Ayele, G.T et al., 2018). This shift is crucial for understanding the dynamic nature of land use and cover, especially in areas affected by environmental disturbances such as floods. Further studies have highlighted the significance of integrating various vegetation indices for more accurate change detection. For example, Liu et al. (2023) reviewed different methodologies for land use change detection, emphasizing the importance of using time-series datasets like NDVI for effective monitoring. The integration of Landsat time-series vegetation indices has further improved the consistency and accuracy of change detection models, as highlighted by recent studies (Waylen et al., 2014; Gao et al., 2005).

There are a dearth of comprehensive research and integrated approaches for assessing the extent of harm to fragmented land cover categories. Considering that flash floods in mountainous regions yield significant and devastating consequences, especially within protected areas (Island et al., 2014; Biswas et al., 2023), it is imperative to investigate the resources and disruption affecting vegetation and other land-use groups within the Central Zagros region (Modrick et al., 2015) Recent studies have shown that land-use changes, such as increased urbanization and deforestation, exacerbate the frequency and intensity of flash floods. For instance, in the Yesanpo scenic national park, land-use changes have heightened the risk dynamics associated with flash floods, leading to considerable property damage and disruption of local ecosystems (Chen et al., 2020). In the Central Zagros region, the interplay between vegetation growth, land cover dynamics, and increasing water scarcity further complicates the situation. Changes in vegetation cover can either mitigate or exacerbate the effects of flash floods depending on the nature of the changes (Behling et al., 2022).

This study aims to examine the effects of floods on land-use/land-cover (LULC) patterns and transitions in the SPA, a biodiversity hotspot and a cultural heritage site in Central Zagros, Iran. Using fragmentation analysis and LULC change detection, and comparing them with landscape pattern indices, the study investigates how floods affect the spatial characteristics and processes of different LULC types in the short term. Landscape measurement tools are utilized to assess the spatial organization of patches, land classes, or entire mosaics across a landscape. The study evaluates the impact of floods on land cover using fieldwork and interviews, which collect data and information from the ground and the local people. It hypothesizes that floods have a significant negative effect on the LULC patterns and transitions, especially on Farmlands and Barre lands, and that the vulnerability and resilience of different LULC types depend on their characteristics and processes. The study provides valuable evidence for response planning and mitigation of future flood events, enhancing the resilience and adaptation of the study area to flood hazards and climate change. By understanding the interplay between flooding events and land cover changes, we aim to inform better land management practices and policy-making that can mitigate the adverse effects of floods while leveraging their ecological benefits.

## 2 Materials and methods

### *2.1 Study area*

This research focused on the Sefid Kuh Protected Area (SPA), with an area of 70,031 hectares, which is administered by the Department of Environment (DoE) of Lorestan Province and covers parts of Khorramabad and Selseleh in western Iran. It is between latitudes 33°30′01.18′′ and 33°47′40.15′′ N and longitudes 47°57′01.18′′ and 48°14′40.15′′ E and has an elevation that ranges between 1,120 meters and 3,870 meters. For a temperate Mediterranean area, the average annual precipitation and temperature reach up to 600 mm and 11 °C, respectively (Darvishsefat et al., 2006) The majority of the rural population lives at lower elevations alongside rivers (Firouz, 2005). The SPA, recognized as a protected area in 1968 and upgraded to a fully protected area in 1990, is characterized by its mountainous terrain, including the Sefidkuh mountain range, part of the larger Zagros Mountain system. These mountains formed due to the collision of the Arabian and Eurasian tectonic plates, resulting in a complex geological structure with steep slopes, deep valleys, fault lines, and thrusts. Erosional forces, particularly water erosion, have shaped the region into river valleys, gorges, and alluvial fans. The hydrological network, comprising small rivers and streams, plays a crucial role in shaping the area's geomorphology.

The SPA, apart from its geological significance, is an area that has the diversity of rich habitats and supports high numbers of plant and animal species (Noroozi et al., 2020). Thirty-eight animal species from the SPA have been recorded, including, but not limited to, the Persian squirrel, wild goat, brown bear, Persian leopard, and wild cat, evidence of the rich biodiversity of area (Darvishsefat et al., 2006). Field visits showed great damage to land cover within the boundaries of the SPA due to floods and further increased the importance of this protected area as a hotspot for biodiversity in the Central Zagros region (Vaghefi et al., 2019).

Massive floods that hit Lorestan Province in March 2019 made a huge difference. They affected over 1,800 villages, 200 completely submerged and

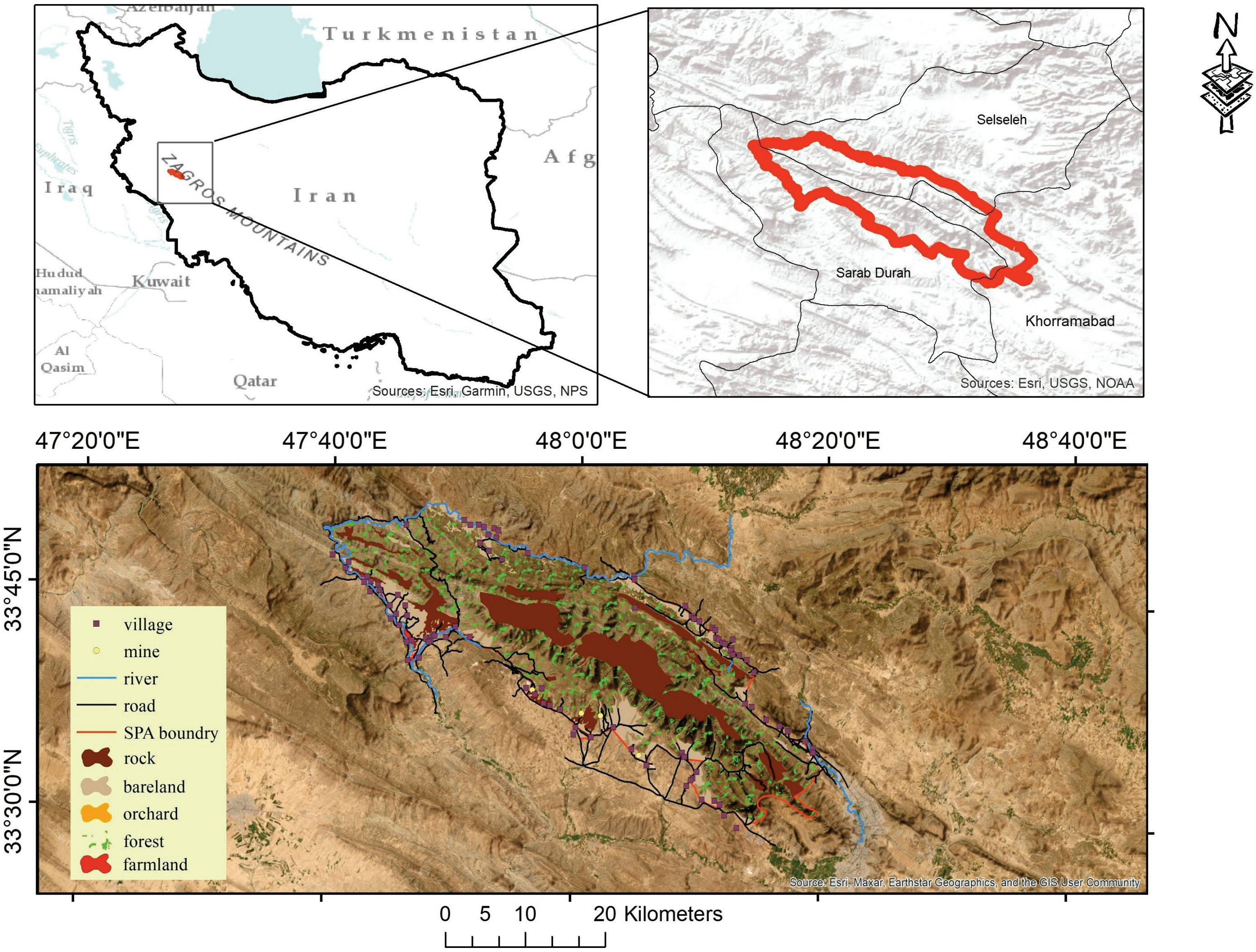


**Figure 1.** The study area is in Lorestan Province, western Iran, highlighting the protected area of SPA in the Zagros Mountains for investigation and modelling.

about 15 people dead. Severely damaged infrastructure included coastal walls, roads, water lines, and cut power. The flooding also had serious effects on health services, agriculture, and cultural heritage centers (SRCIF, 2019). The area faced two major rainfall events: the first, which poured 141 mm from March 23 to 26, 2019, and the latter drenched the area with 181 mm from March 30 to April 1, 2019, leading to 1.35 and 1.3 billion cubic meters of rainfall, respectively (Lorestan Regional Water Company, 2019). The town of Khorramabad incurred the greatest damage to its socio-economic aspects. However, the floods not only devasted Kashkan coastal wall in the Poldokhtar but also resulted in the destruction of residential and commercial areas under floodwaters. Unfortunately, Sarab Durah city suffered similarly with water flooding more than a third of its residential and industrial houses thereby erratically covering residential areas and protected commercial zones (Lorestan Governorate, 2019).

## *2.2 Standardized Precipitation Index (SPI)*

The Standardized Precipitation Index (SPI) is a widely used meteorological drought index (Guttman et al., 1999; Vicente et al., 2010) that quantifies observed precipitation anomalies relative to a selected probability distribution function. It provides a standardized departure from the long-term mean precipitation, allowing comparisons across different regions and climates The SPI values indicate increasingly severe rainfall deficits (droughts) as SPI decreases below -1.0 and excess rainfall as SPI increases above 1.0. Further the SPI represent the number of standard deviations by which the observed anomaly deviates from the mean. The formula for SPI calculation is as follows:

$$SPI=\frac{P - P^*}{\sigma_p}$$

(P) represents the observed precipitation

(P*) is the mean precipitation

($\sigma_p$) is the standard deviation of precipitation

## *2.3. Data Collection*

To assess the extent of damage incurred by five distinct land-use categories, specifically agriculture, snow-covered areas, barre land, compact woodland, and thin woodland, a total of 60 sampling points were collected for each land cover type. The data collection process encompassed 355 points acquired in 2018 before the occurrence of the flood event, with these pre-flood data points collected by environmental experts from the natural resource organization of Lorestan. An additional 362 points were collected post-event in 2019 through field work and expert observations. In this study, a two-time series of LANDSAT 8 satellite imagery from 2018 and 2019 was employed to analyze the changes in land cover. The bands of 4 (red) and 5 (near infrared) from the Landsat 8 data were used to create an NDVI (Normalized Difference Vegetation Index) map to further assess the changes in vegetation. Both time series of satellite imagery underwent an initial rectification and geo-referencing process, aligning them to the Universal Transverse Mercator (UTM) zone 39 projection system, utilizing the World Geodetic System (WGS) 1984 datum. The primary objective of this study was to quantify the variations in flood events between the year of the flood (2019) and the preceding year (2018). The satellite images were sourced from the official website of the United States Geological Survey (USGS) at [earthexplorer.usgs.gov] (Table 1). The acquired satellite images were utilized to conduct a comprehensive analysis of the spatial and temporal changes in land cover classifications within the mountainous region under investigation. To mitigate the potential influence of cloud cover and seasonal variations on the accuracy of the classification process, the images were deliberately captured on dry and clear-sky days toward the conclusion of

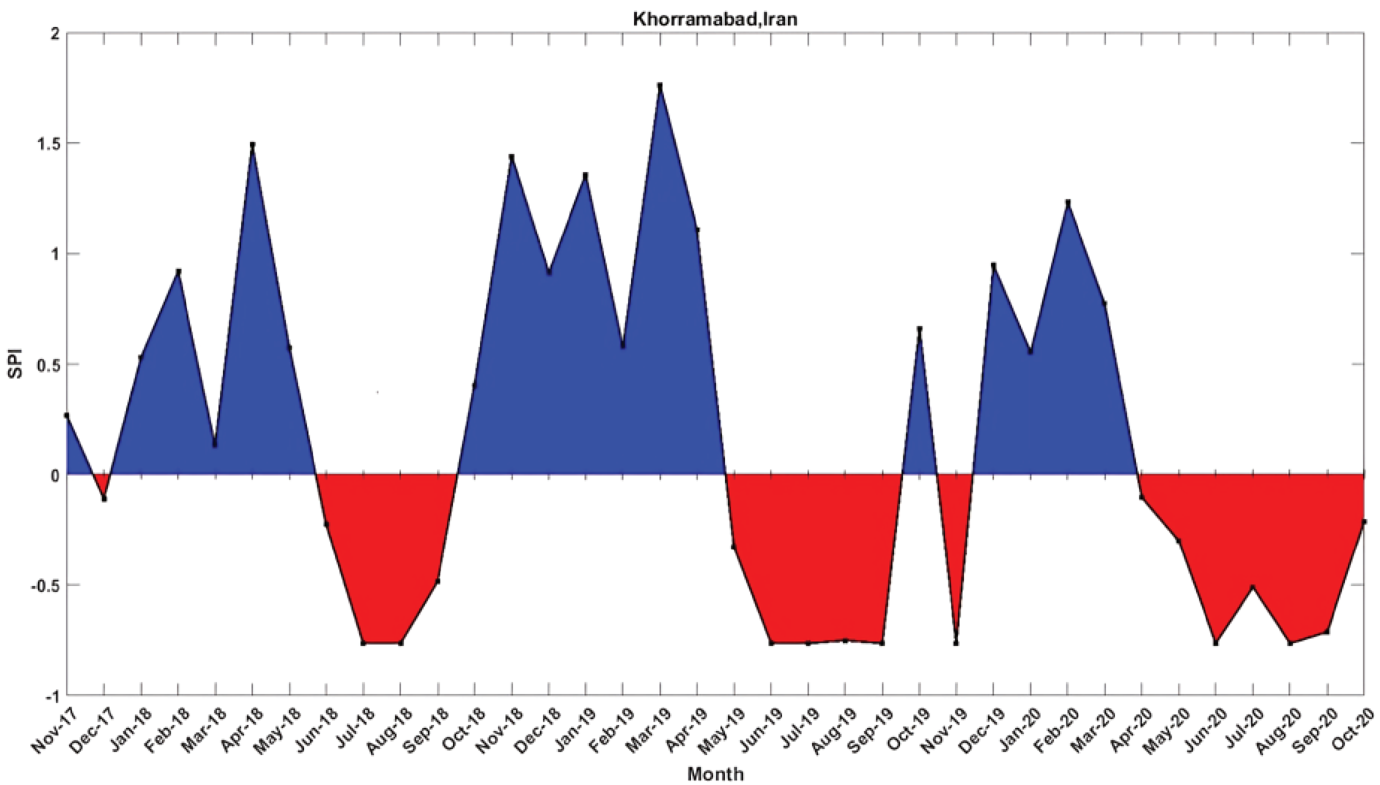


**Figure 2.** 36-monthly SPI (Standardized Precipitation Index) for SPA (2017-2020; (IRIMO 2018)). The blue bars represent positive precipitation, while the red bars indicate negative precipitation values. The data reveals the seasonal variations in the local climate.

**Table 1**. This table provides the details of the Landsat 8 satellite imagery used in this study.

| Scene ID | Sensor | Scene Cloud | No. of Bands | Selected bands | Spatial Resolution | Acquired Date |
|---|---|---|---|---|---|---|
| LC81660372018271LGN00 | Operational Land Imager/ Thermal Infrared Sensor | 0.04 | 11 | B5, B4 | 30*30m | 2018-09-28 |
| LC81660372019290LGN00 | Operational Land Imager/ Thermal Infrared Sensor | 1.15 | 11 | B5,B4 | 30*30m | 2019-10-17 |

the winter season. By employing this approach, the study aimed to enhance the reliability and precision of the land cover classification results.

The methodology employed in this study encompassed three primary stages: preprocessing, processing, and post-processing of the satellite images. To facilitate the implementation of geographic information system (GIS) and remote sensing (R.S.) techniques, a range of software packages were utilized, including ArcGIS 10.3, ERDAS Imagine 2015, and ENVI Classic 2015. Specifically, ENVI Classic (5.3) was utilized for the analysis phase. The acquisition of satellite images was conducted during the autumn season, as vegetation exhibits distinct characteristics during this time, aiding in the differentiation of various ground cover types. While it is ideal to gather images during the summer months (June to August) for the temporal identification of vegetated regions, as suggested by previous studies, the autumn season was chosen in this particular study (Wang et al., 2017).

## *2.4 Data processing*

The preprocessing of the two Landsat images involved standard image processing techniques, including extraction, layer stacking, re-projection, radiometric enhancement, and topographic correction. Considering the temporal and multi-sensor nature of the study, a radiometric adjustment protocol was applied to account for variations in reflectance caused by solar distance and angle differences, utilizing three calibration measures to obtain accurate bottom-of-atmosphere (BOA) reflectance values (Dar et al., 2019; Prieto-Amparan et al., 2018). These measures included the empirical line method (ELM) (Song et al., 2001; Chavez, 1988), which establishes a linear relationship between digital number (DN) values and ground reflectance values by using two reference targets with known reflectance (Ariza, A. et al., 2018). The conversion to BOA reflectance is crucial for minimizing atmospheric effects, thereby providing more reliable data for land use analysis in the SPA (Prieto-Amparan et al., 2018).The ELM method was used for the radiometric correction of the Landsat images, which aims to remove the effects of atmospheric scattering and absorption and to convert the DN values to surface reflectance values. The results of the method were compared and validated using the root mean square error (RMSE) and the coefficient of determination (R2) statistics. The ELM method was found to have the best performance, with the lowest RMSE and the highest R2 values, and was therefore selected for the radiometric correction of the Landsat images.

The equations used (for measuring) the radiance of the at-sensor in W/($m^2$ * sr × µm) are as follows:

Gain= (Lmax-Lmin)/(DNmax-DNmin)

Bias=Lmin-gain×DNmin

Radiance=gain×DN+bias

The calibration constants are Lmax and Lmin, DN is the initial digital numbers of the images, and DNmax and DNmin are the images' digital numbers. The understanding of the workflow for conducting the modeling process is visually presented in Figure 3. through an explanatory flowchart. This diagram illustrates the sequential steps involved in carrying out the modeling tasks, providing a clear and concise representation of the overall process.

## *2.5 Landcover Classification*

The classification of land-use classes was conducted using the Supervised Random Forests (RF) machine learning algorithm after calibrating the two Landsat images. The Supervised Random Forest algorithm, chosen for its effectiveness in land-use classification tasks, applies an ensemble learning approach based on decision trees. It has been widely utilized in remote sensing studies for accurate and efficient classification of land cover (Balha et al., 2023; Talukdar et al., 2020). RF is an ensemble-based classifier

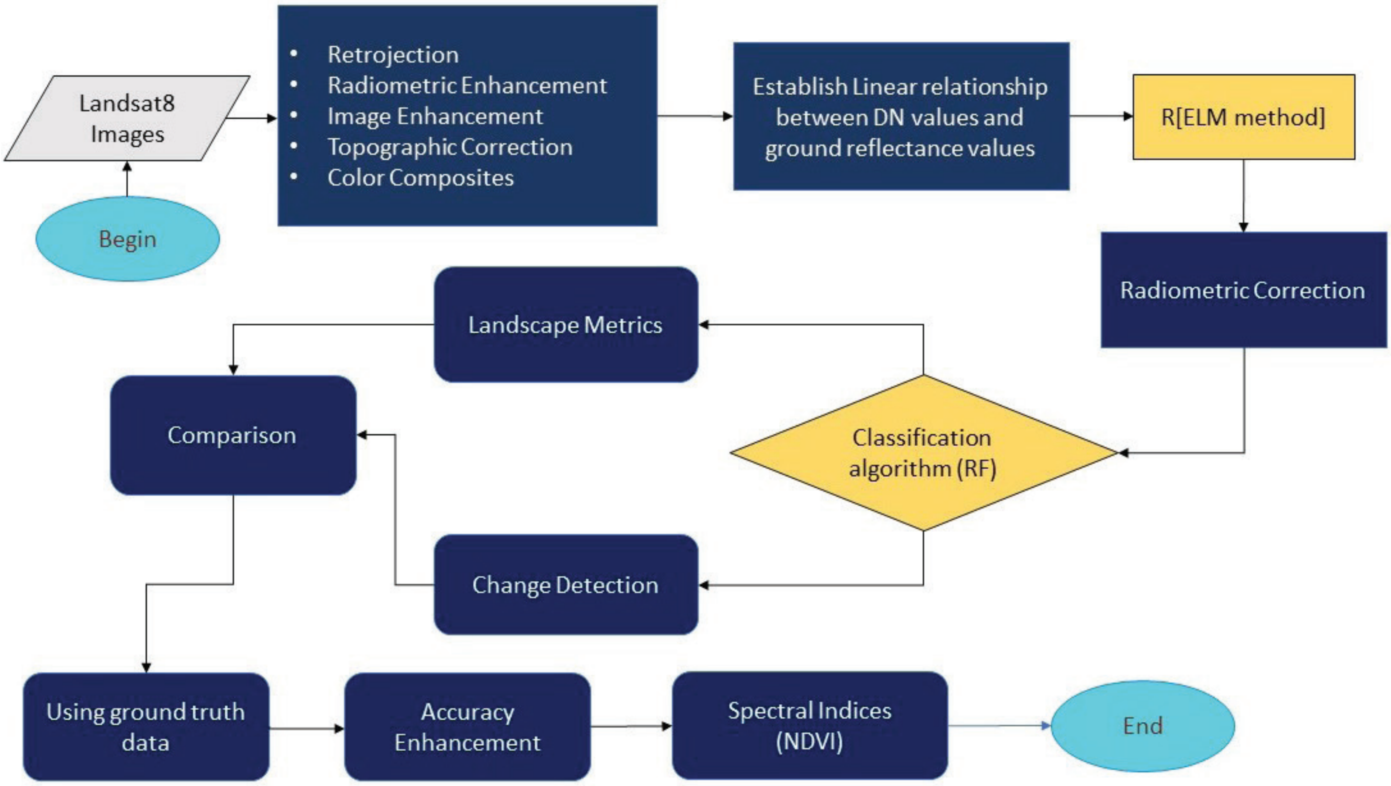


**Figure 3.** Explanatory flowchart illustrating the sequential steps involved in performing the modelling process. This flowchart outlines the key steps in the methodology, including image processing, establishing DN-reflectance relationships, landscape metrics calculation, classification, change detection, accuracy enhancement, and spectral index derivation to analyse land cover changes.

consisting of randomized base regression trees. Each random tree comprises a root node, internal nodes (splits), and terminal nodes at different levels. The root node incorporates all training samples and traverses the tree to determine the optimal split at each node, utilizing a randomly selected subset of input variables. To ensure the representation of all classes in the training data, additional criteria were established to enhance the coherence of the classification outcomes within our specific case study. Extensive scrutiny and analysis were conducted to fulfill these requirements. To facilitate this process, the Differential Vegetation Index of Normalization (NDVI) was introduced, as proposed by previous studies (Huang et al., 2021). NDVI serves as a valuable metric for assessing vegetation dynamics and plays a crucial role in our classification methodology (Ayanlade et al., 2017). The utilization of NDVI within our methodology is attributed to its capacity for discerning vegetation density and condition, rendering it particularly effective for forested mountainous regions. Furthermore, the incorporation of a slope layer has demonstrated a significant enhancement in the accuracy of predictions pertaining to sparsely vegetated or barre areas. Notably, the inclusion of an Euclidean distance measurement to the area's road network layer has proven instrumental in identifying artificial surface classes, as dense road networks are indicative of intensive human activity and altered land use patterns. Subsequently, the consolidation of classes is performed, with a particular emphasis on the fragmentation of LULC. Initially, six distinct land use groups were selected to encompass the diverse land cover in the study area. Given the focus on LULC fragmentation monitoring, the detection of shifts primarily centers on transitions from woodland land cover to sparsely vegetated areas, barre, or artificial land uses (indicative of deforestation), and vice versa (indicating reforestation).

### 2.5.1 Ground Truthing for LULC Classification

To ensure the accuracy and reliability of the LULC classification for the years 2018 and 2019, a comprehensive ground truthing process was conducted. This process involved generating random points within the study area using GIS software. A statistically significant number of points, typically around 300, were selected to cover various land cover categories, including Compact Woodland, Thin Woodland, Rock, Barren Land, Snow, and Farmland. Initially, satellite images and field samples were collected for areas with increasing, decreasing, and constant characteristics. Field data collection was performed by navigating to each randomly generated point using GPS devices. At each location, the actual land cover type was recorded, and photographs were taken for visual documentation and verification purposes. The collected ground truth data was then integrated into the GIS system to create a confusion matrix, which is essential for assessing classification accuracy. The matrix allowed for the calculation of several key metrics:

### 2.5.2 Producer's Accuracy

It is a measure of omission error, indicating the likelihood that a reference pixel is correctly classified. High Producer Accuracy means that few pixels of the class are omitted from being correctly identified. In mathematical terms, if $N_{correct}$ is the total number of classified points that match the reference data, and $N_{total}$ is the total number of reference points for that class, the formula for Producer's Accuracy is:

$$PA=\frac{N_{correct}}{N_{total}}$$

### 2.5.3 User's Accuracy

the User's Accuracy, also known as the User's Commission, is a measure of the accuracy of a classification map from the perspective of the map user. It's calculated as the number of correctly identified pixels of a given class divided by the total number of pixels that were classified as that class. In mathematical terms, if $N_{correct}$ is the total number of classified points that match the reference data, and $N_{classified}$ is the total number of points that were classified as that class, the formula for User's Accuracy is:

$$\mathrm{UA}=\frac{N_{correct}}{N_{total}}$$

### 2.5.4 Overall Accuracy

The recorded land cover types were matched against the predefined classification categories to ensure consistency. Subsequently, the images underwent evaluation using overall accuracy indices and the Kappa coefficient. The overall accuracy indices were computed using a specific equation:

$$OA=\frac{1}{N}\sum p_{ii}$$

In operational contexts where classification accuracy is compared, the Kappa coefficient index is frequently employed due to the presence of errors in overall accuracy. The Kappa coefficient considers the sum of the main diagonal elements of the error matrix, and it specifically targets pixels that have been classified incorrectly.

### 2.5.5 The Kappa Coefficient

The Kappa coefficient is a statistical measure used to evaluate the agreement between two raters or classifications while accounting for the agreement occurring by chance. It is particularly useful in assessing the accuracy of land cover classifications in remote sensing and thematic mapping.

The Kappa coefficient (K) can be calculated using the following formula (Rwanga et al., 2017):

Po: (Observed Agreement) is the proportion of instances where the raters agree.

Pe: (Expected Agreement) is the proportion of instances that would be expected to agree by chance.

$$K=\frac{P_o-P_e}{1-P_e}$$

Ideally, the value of the Kappa coefficient is one. If this value is equal to zero the classification is completely random and if a negative value is obtained, there is an error in the classification.

To assess the land use and land cover changes between the two time periods, a random sampling approach was used to select 60 reference points, which were then compared to the corresponding map classifications using the Kappa coefficient method.

## *2.6 Change detection*

The objective of this study is to obtain spatial and quantitative information regarding LULC shifts. To achieve this, a post-classification (P.C.) comparison technique, specifically cross-classification, is employed. This analysis facilitates the quantitative assessment of changes and, more importantly, transitions in class information. The pixel-by-pixel approach adopted in this shift analysis enables the measurement of both the extent and spatial distribution of modifications in land cover. By utilizing this methodology, comprehensive insights into the dynamics and patterns of LULC changes can be obtained (Coppin et al., 2004). The P.C. contrast method involves the analysis of two image sequences, each spanning the intervals of 2018 and 2019 (Table S1). The primary objective of this method is to visually portray the LULC changes that took place during the research period. Additionally, it seeks to provide a concise overview of the assigned LULC changes categories and explore potential correlations with relevant events. From a quantitative perspective, the resulting transformation maps effectively illustrate the periodic LULC changes that occurred during both the flooded and non-flooded periods.

The WGS 84/UTM Zone 39N spatial reference method was employed to acquire precise GPS coordinates within the protected area. These coordinates were utilized in executing the Maximum Likelihood algorithm, enhancing the accuracy of the monitored classification. Furthermore, the obtained GPS coordinates were instrumental in assessing the study's overall precision.

To quantify the changes that transpired after the flood, the rate of change was calculated using a specific formula. This formula, based on the equation [1]:

$$[1]\ \text{Rate of change (\%)} = \left[\left(\frac{a1}{a2}\right)^{1/n} -1\right] \text{X } 100$$

(FAO, 1995, Gregorio, 2005)

*A1= Basic year data (previous)*

*A2= Last year's data (new)*

*N= Number of years*

## *2.7 Landscape metrics*

Landscape indices provide a valuable means of estimating land elements and classes, with their interpretation dependent on the scale and spatiotemporal resolution (Walz, 2008; Herzog & Lausch, 2001). In this study, the SHDI index, widely used to measure diversity in ecological communities (McGarigal, 2000), was employed to assess land use diversity in the landscape before and after the flood. This index examines the types and proportions of land use categories during the specified periods. The Shannon/Weaver index, which ranges from 0 to 1, reflects the level of diversity in the landscape. A value of 0 indicates a landscape consisting of a single biotope type, indicating no diversity.

$$H' = -\sum_{i=1}^{n} p_i \, lnp_i$$

where ($n$) is the number of elements in the system, and ($pi$) is the proportion of the i-th element. The proportion is calculated by dividing the frequency or abundance of the element by the total frequency or abundance of all elements.

As the number of different biotope types or the proportional distribution of area among patch types increases, the index value increases, signifying a greater degree of fairness or heterogeneity. However, it is important to note that this index can be influenced by natural events such as floods, which can alter the distribution and composition of biotope types (Bogaert, 2001). This study focuses on quantitatively investigating the magnitude of land use changes caused by such natural events, specifically examining whether these changes increase or decrease. The Interdispersion and Juxtaposition Index (IJI) (McGarigal & Marks, 1995) is utilized to assess the heterogeneity of biotopes and patch types. In this study, the IJI was calculated at the landscape level. This specification also applies to all the metrics included in Tables 3 and 4, where each metric was calculated at the landscape level. accordingly. The Interdispersion- and Juxtaposition-Index (IJI) is utilized to assess the heterogeneity of biotopes and patch types. When the IJI value approaches 0, it indicates a less even distribution of patch adjacencies, implying less interspersion and juxtaposition within the biotope. Conversely, a value close to 100 suggests a more even distribution of patch adjacencies, indicating higher interspersion and juxtaposition (Farina, 2000). These indicators were calculated using the FRAGSTATS (McGarigal, 2000) network-based spatial pattern analysis program. Several metrics were used to calculate these landscape indices, including class level measurement, area percentage, number of patches, Total Edge, landform shape, largest spot, average spot level, and average Euclidean distance. The definitions and equations for each metric can be found in Table S1 and Table S22 of this study. By incorporating landscape indices and their associated metrics, this research aims to provide a comprehensive understanding of the spatial patterns, diversity, and heterogeneity of land use within the study area. These analyses contribute to a more nuanced assessment of the impacts of the flood and provide insights for effective land management and planning strategies.

## 3 Results

### *3.1. Comparing LULC change in two years*

Both Figure 4-a. and Figure 4-b. illustrate the land-use classification in 2018 and 2019, showcasing the trend of changes resulting from flood events on land-use classes. In 2018, the compact and thick Woodland

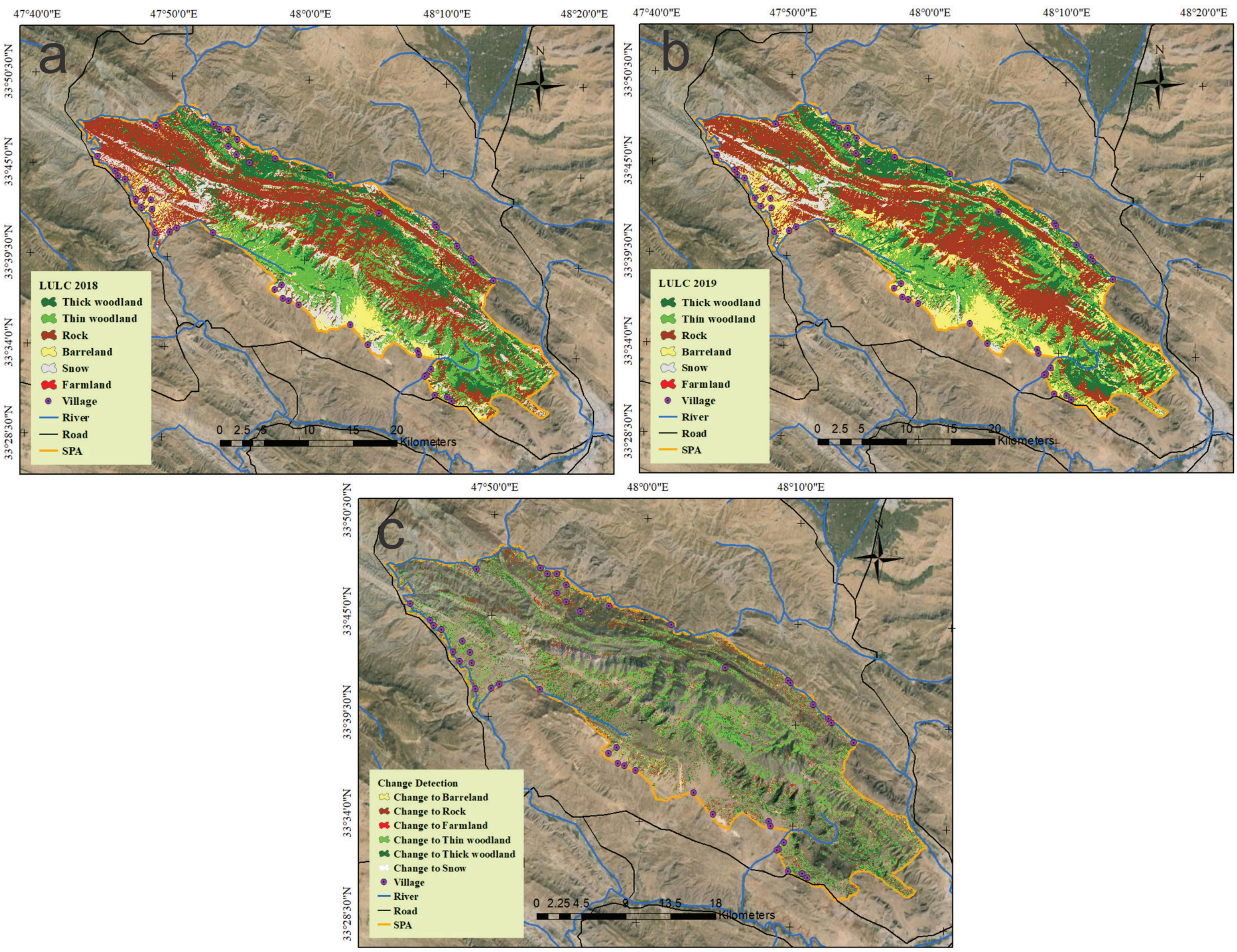


**Figure 4.** The Land Use and Land Cover Map of the Study Area. This thematic map shows the spatial distribution of land cover types such as Thick Woodland, Thin Woodland, Rock, Barreland, Snow, Farmland, and Village, as well as the river network and road infrastructure within the study region. (a: Land Use and Land Cover Map of 2018, b: Land Use and Land Cover Map of 2019). C: land use and land cover (LULC) change detection between the years 2018 and 2019.

encompassed 13,643 and 13,918 hectares respectively. However, in 2019, these figures decreased to 14,473 and 11,115 hectares respectively, indicating a rise in the proportion of compact Woodland as a result of the flood, while thin Woodland decreased after the flooding. This increase is primarily based on the NDVI values indicating an increase in greenery (Brown & Davis, 2021). Tables 2 and 3 demonstrate the high accuracy of these findings, with an overall accuracy of 90% for the points prepared by experts in the 2018 classification, and approximately 91% in 2019. Focusing on changes in agriculture, there was a significant decrease during the flooding period, with this class declining from 303 hectares to 153 hectares. Other classes, such as snow, experienced a sharp decrease from 10,242 hectares to 5,635 hectares. The Rock class also exhibited a decline from 26,487 hectares to 25,634 hectares, possibly due to woody debris flowing onto rocky areas. Another notable change pertains to Barreland, which experienced an increase from 5,430 hectares to 13,014 hectares during the given period. This increase can be attributed to the transformation of other land uses into Barreland (Mandala et al., 2024). A comparison of land-use classes in SPA reveals a significant difference between the two years before and after the flooding, as presented in Table 4. The highest amount of change is observed in the Barreland class, which amounts to 10.83%. The map presented in Figure 4-c. provides a comprehensive spatial analysis of land cover changes within the study area over the observed short period. The map delineates various types of land cover changes, including conversions to and from Barreland, rock, farmland, thin woodland, thick woodland, and snow cover.

The two-way diagram of land use changes from 2018 to 2019 revealed significant dynamics in our study area. Notably, the most substantial change occurred in barre regions, while snowy areas experienced the

**Table 2**. The confusion matrix and accuracy assessment metrics for the 2018 land cover classification. It shows the producer's and user's accuracy for each land cover class, as well as the overall classification accuracy and the Kappa coefficient. The table provides a detailed breakdown of the classification performance, including the commission and omission errors for each class.

| | | Ground truth | | | | | | Total | Commission error (%) | Omission error (%) |
|---|---|---|---|---|---|---|---|---|---|---|
| | | **Compact Woodland** | **Thin Woodland** | **Rock** | **Barreland** | **Snow** | **Farmland** | | | |
| *Classification* | Compact Woodland | 54 | 0 | 1 | 1 | 3 | 1 | 60 | 10 | 1.66 |
| | Thin woodland | 0 | 57 | 1 | 2 | 0 | 0 | 60 | 5 | 10 |
| | Rock | 0 | 3 | 57 | 0 | 0 | 0 | 60 | 5 | 10 |
| | Barreland | 0 | 0 | 3 | 49 | 1 | 2 | 55 | 10.9 | 10.90 |
| | Snow | 1 | 0 | 2 | 3 | 53 | 1 | 60 | 11.66 | 8.33 |
| | Farmland | 0 | 3 | 1 | 0 | 1 | 55 | 60 | 8.33 | 6.66 |
| Total | | 55 | 63 | 65 | 55 | 58 | 59 | | | |
| Producer accuracy | | 94 | 87 | 94 | 90 | 86 | 92 | Kappa coefficient: 89.36 | | |
| User accuracy | | 85.45 | 83.21 | 92.15 | 90 | 93.47 | 97.87 | Overall accuracy: 0.90 | | |

**Table 3**. The confusion matrix and accuracy metrics for the 2019 land cover classification. It includes producer's and user's accuracies for each class, as well as the overall accuracy and Kappa coefficient. The table details the commission and omission errors for the different land cover types.

| | | Ground truth | | | | | | Total | Commission error (%) | Omission error (%) |
|---|---|---|---|---|---|---|---|---|---|---|
| | | **Compact Woodland** | **Thin Woodland** | **Rock** | **Barreland** | **Snow** | **Farmland** | | | |
| *Classification* | Compact Woodland | 54 | 0 | 1 | 1 | 3 | 1 | 60 | 10 | 1.82 |
| | Thin woodland | 0 | 57 | 1 | 3 | 0 | 0 | 61 | 6.56 | 12.31 |
| | Rock | 0 | 3 | 56 | 0 | 1 | 0 | 60 | 6.67 | 11.11 |
| | Barreland | 0 | 2 | 2 | 53 | 1 | 2 | 60 | 11.67 | 11.67 |
| | Snow | 1 | 0 | 2 | 3 | 55 | 0 | 61 | 9.84 | 9.84 |
| | Farmland | 0 | 3 | 1 | 0 | 1 | 55 | 60 | 8.33 | 5.17 |
| Total | | 55 | 65 | 63 | 60 | 61 | 58 | | | |
| Producer accuracy | | 90 | 95 | 95 | 81.66 | 88.33 | 91.66 | Kappa coefficient: 89.36 | | |
| User accuracy | | 90 | 95 | 95 | 89.09 | 88.33 | 91.66 | Overall accuracy: 0.90 | | |

**Table 4**. The confusion matrix and accuracy metrics for the 2019 land cover classification. It includes producer's and user's accuracies for each class, as well as the overall accuracy and Kappa coefficient. The table details the commission and omission errors for the different land cover types.

| | Area in ha | | Area Change | Area in Percent | | Change (%) | a1/a2 | a2/a1 | Percentage of changes |
|---|---|---|---|---|---|---|---|---|---|
| **Name** | 2018 | 2019 | 2018 to 2019 | 2018 | 2019 | | 2018 to 2019 | | |
| **Compact Woodland** | 13643 | 14473 | 830 | 19.48 | 20.66 | 1.18 | -2.89774 | 2.98422 | 6.057495 |
| **Thin Woodland** | 13918 | 11115 | -2803 | 19.87 | 15.87 | -4 | 11.89495 | -10.6305 | -20.1309 |
| **Agriculture** | 303 | 153 | -150 | 0.43 | 0.21 | -0.22 | 43.09504 | -30.1164 | -51.1628 |
| **Snow** | 10242 | 5635 | -4607 | 14.62 | 8.04 | -6.58 | 34.84836 | -25.8426 | -45.0068 |
| **Rock** | 26487 | 25634 | -853 | 37.82 | 36.60 | -1.22 | 1.653005 | -1.62612 | -3.22581 |
| **Barreland** | 5430 | 13014 | 7584 | 7.75 | 18.58 | 10.83 | -35.4155 | 54.83602 | 139.7419 |

largest decrease. These alterations were likely influenced by various factors, including natural events such as floods. (Table 4) provides further insights into these land use changes. Specifically, agriculture showed the lowest percentage of change, suggesting relative stability in agricultural land cover. In contrast, barre land exhibited the highest percentage of change, indicating significant alterations. Barre regions may have been affected by flood-induced erosion or other processes.

Considering downstream effects, sediment transport plays a crucial role in shaping river systems. The flood event likely mobilized sediments, leading to downstream deposition. Understanding sediment pathways and their impact on river ecosystems is vital for sustainable land management. Sediment deposition downstream can influence water quality, aquatic habitats, and channel morphology. It may contribute to the formation of new landforms (e.g., riverbanks, deltas) or affect existing ones. Benefits include nutrient enrichment (essential for riparian vegetation and aquatic ecosystems), land building (fertile floodplains), and habitat creation. However, challenges such as erosion control, navigation hindrance, and flood risk must be considered.

### *3.2 Landscape metrics*

This analysis utilized multiple metrics, including LPI, NP, CA, PLAND, ED, LSI, Split, and TE, to examine the highly detrimental consequences of flood interference on different land cover classes during the study period. Landscape metrics were employed to provide insights into the spatial structure of the evolving landscape (Brown et al., 2021). The CA and PLAND values (Table 5) illustrate the proportion of different land-use classes in hectares and percentages. Both figures demonstrate that all classes, except compact Woodland and Barreland, experienced decreases.

The NP metric indicates the number of patches of a given class and measures the degree of class fragmentation. Values equal to or greater than 1 suggest that the landscape consists of multiple patches. The number of patches shown in Table 5 increased for both woodland classes, with the Barreland class experiencing the largest increase in 2019, around 9,000 patches, while other classes such as Rock, White area, and farmland exhibited decreasing trends. Table 5 displays the patch density, where a lower density implies less fragmented classes. The Barreland class demonstrated the most significant change in density, with a value of 13.1308 per 100, while farmland had the lowest density at 0.7926 percent.

The LPI index (Table 5) measures the percentage of total landscape area occupied by the largest-size patch of a class. A higher value indicates a larger margin length, measured in meters. The most notable change in the LPI index was observed in the Rock class, increasing from 18.34 in 2018 to 26.24 in 2019. Additionally, the Total Edge (TE) metric, representing the absolute length of the entire margin of a class, exhibited a substantial change in the Barreland class. In 2018, it measured 2,306,970 meters, while one year after the flooding, it doubled to 4,770,570 meters (Table 5). Conversely, the snow cover of the region, classified as the White area, decreased from 3,618 hectares in 2018 to 2,332 hectares in 2019.

The Edge Density (ED) metric (Table 5) reflects the shape complexity and spatial heterogeneity of a class. Notable differences were observed after the flooding, particularly in the Barreland class, which increased from 32.98 in 2018 to 68.12 in 2019. In

**Table 5**. Landscape metrics in 2018 and 2019.

| | | Compact Woodland | Thin Woodland | Rock | Barreland | Snow | Farmland |
|---|---|---|---|---|---|---|---|
| **CA (ha)** | 2018 | 13.64 | 13.9 | 26.49 | 5.43 | 10.24 | 0.3 |
| | 2019 | 14.47 | 11.12 | 25.63 | 13.01 | 5.64 | 0.15 |
| **PLAND (%)** | 2018 | 19.48 | 19.88 | 37.83 | 7.76 | 14.63 | 0.43 |
| | 2019 | 20.67 | 15.87 | 36.61 | 18.58 | 8.05 | 0.22 |
| **NP** | 2018 | 5698 | 5711 | 6301 | 6545 | 6456 | 729 |
| | 2019 | 6498 | 6911 | 5674 | 9195 | 5666 | 555 |
| **PD (no./100 ha)** | 2018 | 8.14 | 8.16 | 9 | 9.35 | 9.22 | 1.04 |
| | 2019 | 9.28 | 9.87 | 8.1 | 13.13 | 8.09 | 0.79 |
| **LPI (%)** | 2018 | 3.11 | 4.85 | 18.35 | 1.66 | 1.06 | 0.03 |
| | 2019 | 4.17 | 3.87 | 26.25 | 3.16 | 0.52 | 0.01 |
| **TE (m)** | 2018 | 3901500 | 4220250 | 5288490 | 2309670 | 3618870 | 185400 |
| | 2019 | 4178430 | 4179510 | 4480380 | 4770570 | 2332620 | 116430 |
| **ED (m/100 ha)** | 2018 | 55.72 | 60.27 | 75.52 | 32.98 | 51.68 | 2.65 |
| | 2019 | 59.67 | 59.69 | 63.98 | 68.13 | 33.31 | 1.66 |
| **LSI** | 2018 | 83.78 | 89.75 | 81.88 | 80.34 | 91.39 | 29.08 |
| | 2019 | 87 | 99.46 | 70.33 | 106.23 | 80.78 | 24.67 |
| **IJI (%)** | 2018 | 74.42 | 80.92 | 85.06 | 87.47 | 83.34 | 91.83 |
| | 2019 | 77.88 | 76.87 | 84.19 | 86.61 | 79.24 | 91.81 |
| **Split** | 2018 | 430.02 | 339.4 | 24.22 | 3139.57 | 3304.51 | 4077322.6 |
| | 2019 | 357.06 | 621.55 | 14.44 | 722.79 | 11370.93 | 15176861 |
| **AI (%)** | 2018 | 78.68 | 77.36 | 85.06 | 67.52 | 73.11 | 50.36 |
| | 2019 | 78.47 | 71.9 | 86.98 | 72.24 | 67.95 | 41.01 |
| **Shannon Diversity Index** | 2018 | -0.32 | -0.32 | -0.37 | -0.2 | -0.28 | -0.02 |
| | | -0.33 | -0.29 | -0.37 | -0.31 | -0.2 | -0.01 |

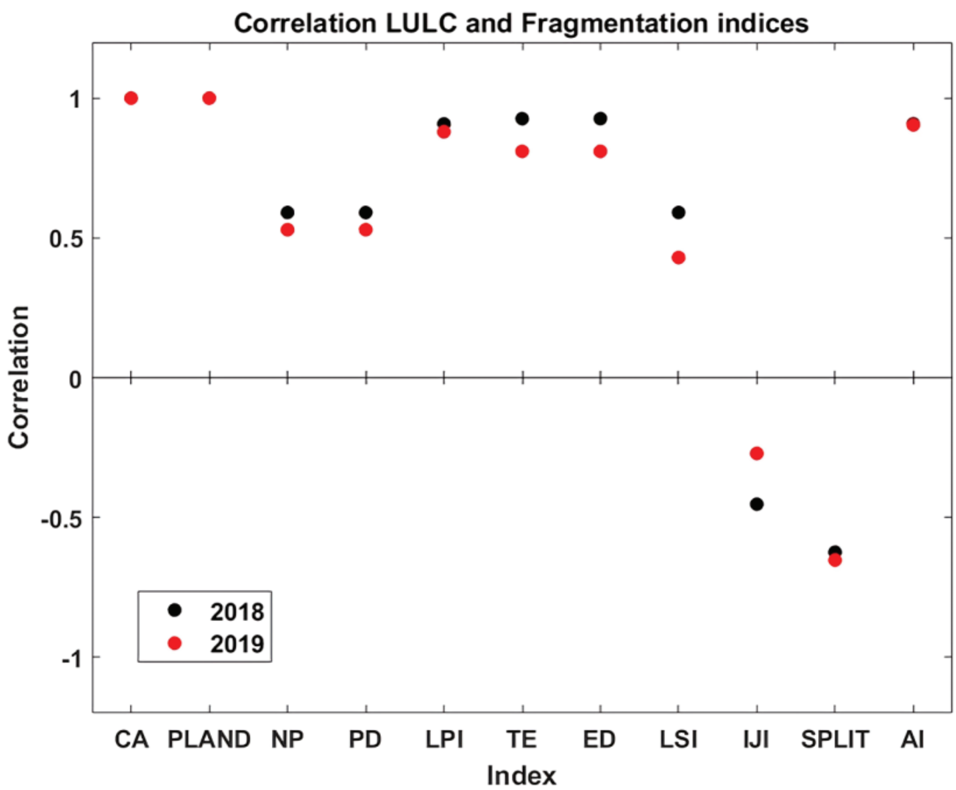


**Figure 5.** Correlation between LULC and Fragmentation Indices from 2018 to 2019. This graph illustrates the relationship between various landscape metrics, including Contagion (CA), Patch Density (PD), Largest Patch Index (LPI), Total Edge (TE), Interspersion and Juxtaposition Index (IJI), and Splitting Index (SPLIT), across two time periods, 2018 and 2019. The correlation values are plotted, allowing for the comparison of these spatial pattern indices and their changes over the one-year interval.

contrast, the White area and farmland exhibited different trends, with values of approximately 51.67 and 2.64 in 2018, and 33.31 and 1.66 in 2019, respectively. The LSI index (Table 5) measures the complexity of a class based on the maximum aggregation of patches within that class. Both woodland classes demonstrated an increase (87.00 and 99.45, respectively) following the flood event, while the Barreland class exhibited the most substantial increase, from 80.33 in 2018 to 106.23 in 2019. Conversely, classes such as farmland, snow cover, and Rock showed decreases (24.67, 80.78, and 70.32, respectively).

The Splitting Index (Table 5) represents the number of equal-sized patches of a particular class required to produce a desired degree of the landscape fragmentation. Notably, significant changes occurred in the farmland class, increasing from 4 hectares in 2018 to 15 hectares in 2019 (Table 5). The isolation and compactness of classes are depicted in Table 5, where lower values indicate higher fragmentation. In this figure, the lowest values were observed for farmland, snow cover, and thin Woodland in 2019 (41.00, 67.95, 71.89, respectively).

The Shannon diversity index values for different land cover types across 2018 and 2019 demonstrate varying diversity trends (Table 5). Compact Woodland and Thin Woodland saw slight decreases in their indices, from approximately 0.31 to 0.30 and 0.31 to 0.29, respectively. Rock experienced a minor decline from 0.34 to 0.33, indicating relatively stable yet slightly reduced diversity. Conversely, Barreland significantly increased its index from about 0.19 to 0.29, suggesting improved biodiversity. Snow exhibited a modest rise from 0.21 to 0.23, while Farmland, despite remaining the least biodiverse category, saw a small increase from approximately 0.02 to 0.03. These results reflect diverse ecological dynamics, with some habitats experiencing declines in species diversity and others showing improvements.

The Pearson's correlation coefficient test conducted to compare the accuracy of estimates of both LULC and Fragmentation methods in assessing land-use changes caused by the flood revealed strong correlations between the two methods in several indices. Specifically, the test demonstrated that the estimates of both methods in the following indices were very similar and correlated with each other Figure 5.

## 4 Discussion

This research focused on how the Random Forest learning method was used to find land cover changes in a short time in the central Zagros Mountains area after the flood in 2019. Wing et al. (2017) are a good example of this method which highlights LC changes when the flood started and tracking them for one year shows land uses that are sensitive right after the flood happens. Zhao's et al. (2020) mentioned how quick decisions are needed after natural disasters also stating that using supervised classification for quick reviews makes sense since it gives clear and correct details about land cover changes which matter for looking at things right after the disaster occurs. An increase in the thick woodland class, shown by higher NDVI values, and the growth in bare lands values related natural changes after floods. These shifts align with what Gabriels et al. (2021) study, which showed land use changes after floods. Goodarzi et al. (2019) reported that undergoing dieback because of stress makes trees more vulnerable to pests and diseases. In places with waterlogged lands and woodlands, this link between stress from nature and insect outbreaks has been shown by Coalson et al. (2021), highlighting the necessity of taking both short- and long-term ecological effects into account when managing post-disaster landscapes (Jones et al., 2022). Size-reduced and fragmented habitats may lead to a decline in species movement and genetic exchange, thus increasing the likelihood of local extinction (Haddad et al., 2015). Conversely, the greater aggregation and clustering of exposed soil areas suggest an elevated risk of erosion and a reduction in habitat availability for native species. Such changes reflect broader shifts in landscape integrity, which have implications for ecological stability and the survival of species within the impacted areas. This degradation aligns with recent research that reports similar declines in ecosystem health and habitat diversity resulting from alterations in land cover and occurrences of flooding (Kayitesi et al., 2022).

Lower values in Shannon's Habitat Diversity Index (SHDI) imply increased habitat fragmentation and degradation, reflecting a decreased complexity and variety of land cover classes (Almenar et al., 2019). The proliferation of fragmentation and isolation in woodland patches, as demonstrated by metrics such as the Largest Patch Index (LPI) and Edge Density (ED), corresponds with patterns identified in recent research that underscore how habitat fragmentation disrupts species connectivity and increases extinction risks (Liu et al., 2019). The aggregation and clustering of bare soil patches suggest greater erosion potential and diminished habitat availability, mirroring broader impacts documented in recent studies regarding land cover changes and their ecological repercussions (Rane et al., 2023).The reduction of dense forests leads to the disappearance of habitats for numerous species that depend on these ecosystems, including the brown bear (*Ursus arctos*), wild goat (*Capra aegagrus*), Persian squirrel (*Sciurus anomalus*), and wild boar (*Sus scrofa*) (Noroozi et al., 2018), which may experience population declines or even local extinction. Such changes also impede ecosystem services; for example, the removal of trees and vegetation diminishes soil stability, making the region more vulnerable to erosion and resulting in sediment accumulation in adjacent water bodies. Furthermore, the absence of tree roots, which function as natural water filtration systems, decreases the area's capacity to purify water, potentially leading to a deterioration in water quality. Additionally, forests serve as carbon sinks, sequestering carbon within their biomass and soils. The conversion of these regions into desolate landscapes eliminates this carbon storage capability, thereby increasing atmospheric carbon levels and intensifying climate change. As a result, shifts in land cover have significant consequences for both biodiversity and critical ecosystem functions. In light of these also future research directions, it is essential to implement continuous monitoring due to potential long-term effects; by systematically tracking changes in land cover and ecosystem health, a more comprehensive understanding of these transformations and their implications can be attained.

Ground-truth data, a critical deficiency combined with satellite image temporal resolution, is a potent influence conceivable, but inferring on LULC change identification and scrutiny. Taken from satellites, these images are set at intervals for analysis purposes. Ground-truth data is also an impediment to our LULC change detection, confounding and restricting classifications. In its absence, a bigger threat of misclassification surfaces; complex sceneries exacerbate the risk of varied landscapes. Regions with scarce forest cover could categorically be misidentified as barren lands. Alternatively, drawing incorrect conclusions on gradual degradation or the genuine scale of deforestation is an opposite scenario. Results emerging from the study we originally carried out have led us to propose several actions for implementation. It would be crucial to establish massive re-planting initiatives as they might bolster the canopy cover. In addition, rooting systems strengthened by such initiatives could maybe mitigate runoff from the surface and help in soil erosion, decreasing during floods, another point of significant import is the application of techniques to reinforce the soil's structure such as planting vegetation possessing long roots or attempting bioengineering methods. These practices could have an impact on preventing landslides. Approaches involving the construction of mitigating zones on riverbanks, flood floodplains are worth considering too. They serve as water storage tanks of excess water, although they might reduce flood pace and offer safety against destruction caused due to floods. A strategy of this nature, particularly when it's paired up with the aspect of safeguarding nearby lands, holds the potential, and could protect the penetrations of floodwater. This kind of association would align with certain land governance principles that advocate for sustainability, as well as tampering down the financial burdens resulting from natural catastrophes that happen repeatedly. The changing climate has resulted in an upward shift in the frequency and severity of natural disasters (IPCC, 2021). A proposal by (Banholzer et al., 2014), recognized the pressing need for pragmatic management strategies during times of crises. A couple of methods were cited, they included the integration of ground-observational data into the assessments for crucial decision-making processes, the bolstering of early warning systems, and the promotion of inter-collaboration among various stakeholders.

## 5 Conclusions

A thorough and detailed investigation was undertaken to analyze changes in LULC by employing fragmentation indices specifically in mountainous regions, focusing on the impactful period before and after the catastrophic floods that struck Iran in 2019. These floods inflicted severe damage on vital infrastructure and essential services, as well as significantly altering various land cover classes in the Zagros Mountain range. The alterations in land cover were particularly striking in SPA, where the repercussions of the flooding were both direct and notably severe. In the aftermath of the flooding, several land cover categories transitioned into barren land, leading to a marked decrease in snow-covered areas and the devastation of delicate woodlands and agricultural zones. Such findings underscore the immediate and profound repercussions that the flooding event had on the regional landscapes, bringing to light the critical impact that natural disasters can impose on the environment. By utilizing landscape pattern indices to assess the structural characteristics of the terrain during the flooding, researchers were able to gain a more precise and nuanced understanding of how various patches within the mountainous landscape were distributed and organized. Among the tools employed, the surface landscape pattern index (LPI) played a pivotal role in quantifying how topographic features influenced landscape patterns, thereby offering a more in-depth comprehension of the interplay between these patterns and the surrounding topography. The significant discrepancies noted between the two years of study lend credibility to the generalizability of the methodological framework applied in this research, suggesting its applicability for evaluating flooding events in similar mountainous regions elsewhere. Furthermore, the trend indicating an increase in agricultural land use on steeper slopes characterized by lower normalized difference vegetation index (NDVI) values points to a widespread shift towards non-irrigated farming, effectively replacing previously forested areas. Notably, the loss of forests exhibited a distinct pattern concentrated on these steeper terrains, attributed to escalating agricultural practices in such high-gradient areas, which may also correlate with rising instances of soil erosion. These intricate observations carry important implications for the planning and management of restoration efforts, emphasizing the need to take into account various biophysical factors inherent to the landscape. The findings from this research particularly highlight the effectiveness of the Random Forest (RF) classification technique when applied to studies focusing on landscape changes in mountainous terrains. The RF method is recognized for its robustness and reliability, being less influenced by the characteristics of different sensors, thus providing a dependable means for accurately analyzing changes in landscapes. As climate change continues to intensify and the frequency and severity of floods increase, addressing the evolving landscape becomes ever more critical. Although native flora and fauna may have historically adapted to natural disturbances, the enhanced environmental stressors resulting from contemporary climate challenges demand proactive intervention. Despite the inherent resilience of these ecosystems, the notable rise in barren lands emphasizes the urgent need for targeted efforts to protect and preserve vegetation. Such initiatives are essential not only for the conservation of biodiversity but also for bolstering the resilience of ecosystems against the backdrop of escalating natural hazards. Acknowledging the shifting dynamics of natural patterns, initiatives like tree planting emerge as proactive strategies to mitigate adverse impacts on both plant and animal species, fostering a more sustainable relationship with the environment.

## Acknowledgements and funding

We would like to express our sincere gratitude to all those who have contributed to this research in various ways. First and foremost, we thank our collaborators and researchers for their invaluable support and guidance throughout the project. Their expertise and insights have enriched our work and made it truly unique. We also acknowledge the resources provided by the Department of Environment (DoE) of Lorestan Province, which enabled us to conduct fieldwork and collect data in a timely and efficient manner. Furthermore, we appreciate the assistance of the Isfahan University of Technology in facilitating our access to relevant literature and databases. Finally, this study was supported by the Slovak Research and Development Agency under the Contract no. APVV-23-0265. This research was also supported by the VEGA agency under the grant number 2/0016/24.

## Declaration of Competing Interest

The authors declare that they have no known competing financial interests or personal relationships that could have appeared to influence the work reported in this paper.

## References


Almenar, J.B., Bolowich, A., Elliot, T., Geneletti, D., Sonnemann, G. and Rugani, B. (2019). Assessing habitat loss, fragmentation and ecological connectivity in Luxembourg to support spatial planning. Landscape and Urban Planning, 189, 335–351. https://doi.org/10.1016/j.landurbplan.2019.05.004

Anderson, B.G., Rutherfurd, I.D. and Western, A.W. (2006). An analysis of the influence of riparian vegetation on the propagation of flood waves. Environmental Modelling & Software, 21(9), 1290–1296. https://doi.org/10.1016/j.envsoft.2005.04.027

Ariza, A., Robredo Irizar, M. and Bayer, S. (2018). Empirical line model for the atmospheric correction of sentinel-2A MSI images in the Caribbean Islands. European Journal of Remote Sensing, 51(1), 765–776. https://doi.org/10.1080/22797254.2018.1482732

Ayanlade, A. (2017). Remote sensing vegetation dynamics analytical methods: a review of vegetation indices techniques. Geoinformatica Polonica, 7–17. https://doi.org/10.4467/21995923GP.17.001.7188

Ayele, G.T., Tebeje, A.K., Demissie, S.S., Belete, M.A., Jemberrie, M.A., Teshome, W.M., Mengistu, D.T. and Teshale, E.Z. (2018). Time series land cover mapping and change detection analysis using geographic information system and remote sensing, Northern Ethiopia. Air, Soil and Water Research, 11, 1178622117751603. https://doi.org/10.1177/1178622117751603

Balha, A. and Singh, C.K. (2023). Comparison of maximum likelihood, neural networks, and random forests algorithms in classifying urban landscape. In Application of Remote Sensing and GIS in Natural Resources and Built Infrastructure Management, 29–38. Cham: Springer International Publishing. https://doi.org/10.1007/978-3-031-14096-9_2

Banholzer, S., Kossin, J. and Donner, S. (2014). The impact of climate change on natural disasters. Reducing disaster: Early warning systems for climate change, 21–49. https://doi.org/10.1007/978-94-017-8598-3_2

Behling, R., Roessner, S., Foerster, S., Saemian, P., Tourian, M.J., Portele, T.C. and Lorenz, C. (2022). Interrelations of vegetation growth and water scarcity in Iran revealed by satellite time series. Scientific Reports, 12(1), 20784. https://doi.org/10.1038/s41598-022-24712-6

Bianchin, S.; Richert, E.; Heilmeier, H.; Merta, M.; & Seidler, C. (2011). Landscape metrics as a tool for evaluating scenarios for flood prevention and nature conservation. Landscape Online, 25(1): 1–15. https://doi.org/10.3097/LO.201125

Billah, M., Masum, M. F. H., & Rana, S. (2023). Random forest classifications for land use mapping to assess rapid flood damage using Sentinel-1 and Sentinel-2 data. Remote Sensing Applications: Society and Environment. https://doi.org/10.1016/j.rsase.2023.100947

Birkeland, P.W.; Colman, S.M.; Burke, R.M.; Shroba, R.R.; & Meierding, T.C. (1979). Nomenclature of alpine glacial deposits, or, what's in a name? Geology, 7(11): 532–536. https://doi.org/10.1016/j.rsase.2023.100947

Biswas, G., Sengupta, A., Alfaisal, F.M., Alam, S., Alharbi, R.S. and Jeon, B.H. (2023). Evaluating the effects of landscape fragmentation on ecosystem services: A three-decade perspective. Ecological Informatics, 77, 102283. https://doi.org/10.1016/j.ecoinf.2023.102283

Bogaert, J. (2001). Landscape Ecology in Action. Landscape and Urban Planning, 53(1–4): 183–184. https://doi.org/10.1007/978-94-011-4082-9

Bolan, S., Padhye, L.P., Jasemizad, T., Govarthanan, M., Karmegam, N., Wijesekara, H., Amarasiri, D., Hou, D., Zhou, P., Biswal, B.K. and Balasubramanian, R. (2023). Impacts of climate change on the fate of contaminants through extreme weather events. Science of The Total Environment, 168388. https://doi.org/10.1016/j.scitotenv.2023.168388

Chalid, A. (2020). Evaluation of flood control in the landuse changess in the Cisangkuy sub-watershed bandung regency, Indonesia, 7(19): 5541–5549. https://doi.org/10.1088/1755-1315/708/1/012029

Chavez, P.S. (1988). An improved dark-object subtraction technique for atmospheric scattering correction of multispectral data. Remote Sensing of Environment, 24(3): 459–479. https://doi.org/10.1016/0034-4257(88)90019-3

Chen, Y., Wang, Y., Zhang, Y., Luan, Q. and Chen, X. (2020). Flash floods, land-use change, and risk dynamics in mountainous tourist areas: A case study of the Yesanpo Scenic Area, Beijing, China. International Journal of Disaster Risk Reduction, 50, 101873. https://doi.org/10.1016/j.ijdrr.2020.101873

Coalson, J.E., Anderson, E.J., Santos, E.M., Madera Garcia, V., Romine, J.K., Luzingu, J.K., Dominguez, B., Richard, D.M., Little, A.C., Hayden, M.H. and Ernst, K.C. (2021). The complex epidemiological relationship between flooding events and human outbreaks of mosquito-borne diseases: a scoping review. Environmental health perspectives, 129(9), 096002. https://doi.org/10.1289/EHP8887

Coppin, P.; Jonckheere, I.; Nackaerts, K.; Muys, B.; & Lambin, E. (2004). Digital change detection methods in ecosystem monitoring: A review. International Journal of Remote Sensing, 25(9): 1565–1596. https://doi.org/10.1080/0143116031000101675

Crossman, N.D., Nedkov, S. and Brander, L. (2019). Water flow regulation for mitigating river and coastal flooding. SEEA EEA Revision, 15.

Croke, J., Thompson, C. and Fryirs, K. (2017). Prioritising the placement of riparian vegetation to reduce flood risk and end-of-catchment sediment yields: Important considerations in hydrologically-variable regions. Journal of Environmental Management, 190, 9–19. https://doi.org/10.1016/j.jenvman.2016.12.046

Dar, I.; Qadir, J.; & Shukla, A.( 2019). Estimation of LST from multi-sensor thermal remote sensing data and evaluating the influence of sensor characteristics. Annals of GIS, 25(3): 263–281. https://doi.org/10.1080/19475683.2019.1623318

Darvishsefat, A.A.; & Tajvidi, M. (2006). Atlas of Protected Areas of Iran. University of Tehran. In persian.

FAO 1995, Gregorio, A. (2005). Land Cover Classification System Classification Concepts and User Manual Software Version (2); Food and Agriculture Organization of the United Nations. Rome, Italy .

Farina, A. (2000). Landscape ecology in action. Kluwer Verlag, Dordrecht . 10.1007/978-94-011-4082-9

Firouz, E. (2005). complete fauna of Iran. IB Tauris. In persian.

Gabriels, K., Willems, P., and Van Orshoven, J. (2022). A comparative flood damage and risk impact assessment of land use changes. Natural Hazards and Earth System Sciences, 22(2), 395–410. https://doi.org/10.5194/nhess-22-395-2022

Gao, L., Zhang, B., Zhang, X. and Li, J. (2005). July. Study on the spectral characteristics of building materials covered by different paint. In Proceedings. 2005 IEEE International Geoscience and Remote Sensing Symposium, 2005. IGARSS'05. 5 : 3208-3211. https://doi.org/10.1109/IGARSS.2005.1526523

Goodarzi, M.; Pourhashemi, M.; & Azizi, Z. (2019). Investigation on Zagros forests cover changes under the recent droughts using satellite imagery. Journal of Forest Science, 65(1): 9–17. https://doi.org/10.17221/61/2018-JFS

Guttman, N.B. (1999). Accepting the standardized precipitation index: a calculation algorithm 1. JAWRA Journal of the American Water Resources Association, 35(2), 311–322. https://doi.org/10.1111/j.1752-1688.1999.tb03592

Haddad, N.M., Brudvig, L.A., Clobert, J., Davies, K.F., Gonzalez, A., Holt, R.D., Lovejoy, T.E., Sexton, J.O., Austin, M.P., Collins, C.D. and Cook, W.M. (2015). Habitat fragmentation and its lasting impact on Earth's ecosystems. Science advances, 1(2), p.e1500052. https://doi.org/10.1126/sciadv.1500052

Hallegatte, S. (2016). Shock waves: managing the impacts of climate change on poverty. World Bank Publications. 10.1596/978-1-4648-0673-5

Herzog, F.; & Lausch, A. (2001). Supplementing land-use statistics with landscape metrics: some methodological considerations. Environmental monitoring and assessment, 72: 37–50. https://doi.org/10.1596/978-1-4648-0673-5

Huang, S., Tang, L., Hupy, J.P., Wang, Y. and Shao, G. (2021). A commentary review on the use of normalized difference vegetation index (NDVI) in the era of popular remote sensing. Journal of Forestry Research, 32(1), 1–6. https://doi.org/10.1007/s11676-020-01155-1

Intergraph. ERDAS IMAGINE (Version 2015) [English; Microsoft Windows]. Hexagon Geospatial. 2015. http://hexagongeospatial.com.

IPCC. (2021). Climate Change 2021: The Physical Science Basis. Contribution of Working Group I to the Sixth Assessment Report of the Intergovernmental Panel on Climate Change. Chapter 11: Weather and Climate Extreme Events in a Changing Climate. Cambridge University Press. https://doi.org/10.1017/9781009157896

Iran Meteorological Organization (IRIMO). (2018). Precipitation Data for Lorestan. Available at: http://www.irimo.ir

Island, W.; Ohimain, E.I.; Izah, S.C.; & Otobotekere, D. (2014). Selective Impacts of the 2012 Water Floods on the Vegetation and Wildlife of Selective impacts of the 2012 water floods on the vegetation and wildlife of Wilberforce Island , Nigeria. (January). https://doi.org/10.11648/j.ijema.20140202.13

Jaeger, J.A.G. (2000). Landscape division, splitting index, and effective mesh size: new measures of landscape fragmentation. Landscape Ecology, 15(2): 115–130. https://doi.org/10.1023/A:1008129329289

Jones, J.A. and Driscoll, C.T. (2022). Long-term ecological research on ecosystem responses to climate change. BioScience, 72(9), 814–826. https://doi.org/10.1093/biosci/biac021

Jönsson, A.M.; Lagergren, F.; & Smith, B. (2015). Forest management facing climate change - an ecosystem model analysis of adaptation strategies. Mitigation and Adaptation Strategies for Global Change, 20(2): 201–220. https://doi.org/10.1007/s11027-013-9487-6

Kayitesi, N.M., Guzha, A.C. and Mariethoz, G. (2022). Impacts of land use land cover change and climate change on river hydro-morphology-a review of research studies in tropical regions. Journal of Hydrology, 615, 128702. https://doi.org/10.1016/j.jhydrol.2022.128702

Lin, W.; Sun, Y.; Nijhuis, S.; & Wang, Z. (2020). Science of the Total Environment Scenario-based flood risk assessment for urbanizing deltas using future land-use simulation (FLUS): Guangzhou Metropolitan Area as a case study. Science of the Total Environment 739: 139899. https://doi.org/10.1016/j.scitotenv.2020.139899

Liu, B., Song, W., Meng, Z. and Liu, X. (2023). Review of Land Use Change Detection—A Method Combining Machine Learning and Bibliometric Analysis. Land, 12(5), 1050.4. https://doi.org/10.3390/land12051050

Liu, J., Coomes, D.A., Gibson, L., Hu, G., Liu, J., Luo, Y., Wu, C. and Yu, M. (2019). Forest fragmentation in China and its effect on biodiversity. Biological Reviews, 94(5), 1636–1657. https://doi.org/10.1111/brv.12519

Lorestan Governorate. (2019). Official response to the request of the Special Committee for the National Flood Report. Available at: https://un-spider.org/sites/default/files/session6-27-arash-malekian-special-remoting-committee-on-iran-floods-2019.pdf

Lorestan Province Crisis Management Coordination Council. (2019). Actions and Activities of the Lorestan Province Crisis Management Coordination Council - April 2019. Available at: https://reliefweb.int/report/iran-islamic-republic/islamic-republic-iran-floods-response-plan-april-2019

Mandala, M., Hakim, F.L., Indarto, I. and Kurnianto, F.A. (2024). Land Use and Land Cover Change in East Java Indonesia from 1972 to 2021: Learning from Landsat. Environmental Research, Engineering and Management, 80(3), 57–69. https://doi.org/10.5755/j01.erem.80.3.35362

McGarigal, K., Cushman, S.A., Neel, M.C. and Ene, E. (2002). FRAGSTATS: spatial pattern analysis program for categorical maps. Computer software program produced by the authors at the University of Massachusetts, Amherst. http://www.umass.edu/landeco/research/fragstats/fragstats.html

McGarigal, K., Cushman, S.A. and Ene, E. (2012). FRAGSTATS v4: spatial pattern analysis program for categorical and continuous maps. Computer software program produced by the authors at the University of Massachusetts, Amherst, 15, 153–162.

McGarigal, K.; & Marks, B.J. (1995). FRAGSTATS: spatial pattern analysis program for quantifying landscape structure. General Technical Report - US Department of Agriculture, Forest Service 351(PNW-GTR-351): 122. https://doi.org/10.2737/PNW-GTR-351

Meurant, M.; Gonzalez, A.; Doxa, A.; & Albert, C.H. (2018). Selecting surrogate species for connectivity conservation. Biological Conservation, 227(September): 326–334. https://doi.org/10.1016/j.biocon.2018.09.028

Modrick, T.M. and Georgakakos, K.P. (2015). The character and causes of flash flood occurrence changes in mountainous small basins of Southern California under projected climatic change. Journal of Hydrology: Regional Studies, 3, .312–336. https://doi.org/10.1016/j.ejrh.2015.02.003

Mostafazadeh, R. and Talebi Khiavi, H. (2024). Landscape change assessment and its prediction in a mountainous gradient with diverse land-uses. Environment, Development and Sustainability, 26(2), 3911–3941. https://doi.org/10.1007/s10668-022-02862-x

Noroozi, J., Talebi, A., Doostmohammadi, M., Rumpf, S.B., Linder, H.P. and Schneeweiss, G.M. (2018). Hotspots within a global biodiversity hotspot-areas of endemism are associated with high mountain ranges. Scientific reports, 8(1), 10345. https://doi.org/10.1038/s41598-018-28504-9

Noroozi, J., Talebi, A. and Doostmohammadi, M. (2020). Plant Biogeography and Vegetation of High Mountains of Central and South-West Asia1. In: J. Noroozi, ed., The Alborz Mountain Range. Plant and Vegetation, vol. 17. Springer Nature Switzerland AG. https://doi.org/10.1007/978-3-30-45212-4_4

Oliver E. J. Wing, Paul D. Bates, Christopher C. Sampson, Andrew M. Smith, Kris A. Johnson, T.A.E. (2017). Validation of a 30 m resolution flood hazard model of the conterminous United States. Water Resources Research. https://doi.org/10.1002/2017WR020917

Paper, D. (2019). Resilient Infrastructure Working Group. Prieto-Amparan, J.A., Villarreal-Guerrero, F., Martinez-Salvador, M., Manjarrez-Domínguez, C., Santellano-Estrada, E. and Pinedo-Alvarez, A. (2018). Atmospheric and radiometric correction algorithms for the multitemporal assessment of grasslands productivity. Remote Sensing, 10(2), 219. https://doi.org/10.3390/rs10020219

Rane, N.L., Achari, A., Choudhary, S.P. and Giduturi, M. (2023). Effectiveness and Capability of Remote Sensing (RS) and Geographic Information Systems (GIS): A Powerful Tool for Land use and Land Cover (LULC) Change and Accuracy Assessment. International Journal of Innovative Science and Research Technology, 8: 286–295. https://www.doi.org/10.56726/IRJMETS38104

Rwanga, S.S. and Ndambuki, J.M. (2017). Accuracy assessment of land use/land cover classification using remote sensing and GIS. International Journal of Geosciences, 8(04), p.611.Saura S, M.-M.J. 2001. Sensitivity of landscape pattern metrics to map spatial extent. Photogram Eng Remote Sense, 67: 1027–1036. https://doi.org/10.4236/ijg.2017.84033

Schaller, N.; Kay, A.L.; Lamb, R.; Massey, N.R.; Van Oldenborgh, G.J.; Otto, F.E.L.; Sparrow, S.N.; Vautard, R.; Yiou, P.; Ashpole, I.; Bowery, A.; Crooks, S.M.; Haustein, K.; Huntingford, C.; Ingram, W.J.; Jones, R.G.; Legg, T.; Miller, J.; Skeggs, J.; Wallom, D.; Weisheimer, A.; Wilson, S.; Stott, P.A.; & Allen, M.R. (2016). Human influence on climate in the 2014 southern England winter floods and their impacts. Nature Climate Change, 6(6): 627–634. https://doi.org/10.1038/nclimate2927

Stolpe, H., Ngoc Ha, N. and Jolk, C. (2022). Regional Water and Land Use Planning: Systematic Planning Support. Water Conservation-Inevitable Strategy. 10.5772/intechopen.102713

Song, C., Woodcock, C. E., Seto, K. C., Lenny, M. P.,& Macomber, S.A. (2001). Classification and change detection using Landdsat TM data. Remote sensing of Environment, 75(2): 230–244. https://doi.org/10.1016/S0034-4257(00)00169-3

SRCIF. (2019). The 2019 Iran Floods Narrative (In Persian).: 44–45 p. Lorestan.

Talukdar, S., Singha, P., Mahato, S., Pal, S., Liou, Y.A. and Rahman, A. (2020). Land-use land-cover classification by machine learning classifiers for satellite observations—A review. Remote Sensing, 12(7), 1135. https://doi.org/10.3390/rs12071135

Tucker, C.J. (1979). Red and photographic infrared near combinations for monitoring vegetation. Remote Sensing of Environment, 8(2): 127–150. https://doi.org/10.1016/0034-4257(79)90013-0

Turner, Monica G., Virginia H. Dale, and R.H.G. (1989). Predicting across scales: theory development and testing. Landscape ecology, 3: 245–252. https://doi.org/10.1007/BF00131542

Vaghefi, S.A.; Keykhai, M.; Jahanbakhshi, F.; Sheikholeslami, J.; Ahmadi, A.; Yang, H.; & Abbaspour, K.C. (2019). The future of extreme climate in Iran. Scientific Reports, 9(1): 1–11. https://doi.org/10.1038/s41598-018-38071-8

Verbesselt, J.; Hyndman, R.; Newnham, G.; & Culvenor, D. (2010). Detecting trend and seasonal changes in satellite image time series. Remote sensing of Environment, 114(1): 106–115. https://doi.org/10.1016/j.rse.2009.08.014

Vicente-Serrano, S.M., Beguería, S. and López-Moreno, J.I. (2010). A multiscalar drought index sensitive to global warming: the standardized precipitation evapotranspiration index. Journal of climate. 23(7), pp.1696-1718. https://doi.org/10.1175/2009JCLI2909.1

Walz, U. (2008). Monitoring of landscape change and functions in Saxony (Eastern Germany)-Methods and indicators. Ecological Indicators, 8(6): 807–817. https://doi.org/10.1016/j.ecolind.2007.09.006

Wang, C.; Chen, J.; Wu, J.; Tang, Y.; Shi, P.; Black, T.A.; & Zhu, K. (2017). Remote Sensing of Environment A snow-free vegetation index for improved monitoring of vegetation spring green-up date in deciduous ecosystems. Remote Sensing of Environment, 196: 1–12. https://doi.org/10.1016/j.rse.2017.04.031

Waylen, P., Southworth, J., Gibbes, C. and Tsai, H. (2014). Time series analysis of land cover change: Developing statistical tools to determine significance of land cover changes in persistence analyses. Remote Sensing, 6(5), 4473–4497. https://doi.org/10.3390/rs6054473

Whited, D.C., Lorang, M.S., Harner, M.J., Hauer, F.R., Kimball, J.S. and Stanford, J.A. (2007). Climate, hydrologic disturbance, and succession: drivers of floodplain pattern. Ecology, 88(4), 940–953. https://doi.org/10.1890/05-1149

Wu, Y.; Li, S.; & Yu, S. (2016). Monitoring urban expansion and its effects on land use and land cover changes in Guangzhou city, China. Environmental monitoring and assessment 188: 1–15. https://doi.org/10.1007/s10661-015-5069-2

Zhao, R.; Liu, X.; & Xu, W. (2020). Integration of coseismic deformation into WebGIS for near real-time disaster evaluation and emergency response. Environmental Earth Sciences 79: 1–11. https://doi.org/10.1007/s12665-020-09153-6

## Supplementary material

Photos of impact of floods in Poldokhtar area of Lorestan (Photograph of Soheyl Moradi) in 2019.08.27

**Table S1**. The descriptions explain the significance of each metric in characterizing the spatial patterns and changes in the land cover classes.

| Landscape Metrics (units) | **Abbreviation** | **Description** |
|---|---|---|
| Patch Density (Number of patches/100 ha) | PD | Lower Density of patches indicates less fragmented classes |
| Edge Density (m/ha) | ED | Indicates the shape complexity and spatial heterogeneity of a class or a landscape class |
| Largest Patch Index (%) | LPI | Percentage of total landscape area occupied by the largest-size patch of a class |
| Aggregation Index(%) | AI | The ratio of the actual edge to the total amount of possible edge. Aggregation index (AI) is the percentage of like adjacencies involving the corresponding patch type, relative to the maximum possible number of like adjacencies. It is calculated by dividing the number of like adjacencies (n_ij) by the maximum possible number of like adjacencies (n_max) and multiplying by 100. AI indicates how clumped or dispersed the patches of the same type are in a landscape. |
| Percentage of land area | PLAND | Percentage of land occupied by a class. The values of this measure vary between 0 and 100, which means zero, which means that the relevant class is increasingly scarce at the land level and one hundred means that the land level consists of only one class |
| Number of Patches | NP | Indicates the number of patches in a given class and measures the degree of class fragmentation. Its values are greater than or equal to 1. When this value is equal to 1, the landscape consists of only one patch of that class |
| Total Edge | TE | The absolute size of the length of the entire margin of a given class. Larger values are equal to one, and the unit is in meters. The total margin is zero when the landscape has no class margin, and the user does not consider any boundary of the land as a margin to be treated. |
| Landscape Shape *Index* | LSI | Measures the complexity of a class relative to the maximum aggregation of patches of that class |
| Splitting Index | Split | The number of equal-sized patches of a particular class required to produce a desired degree of the landscape fragmentation |
| Interdispersion- and Juxtaposition-index | IJI | Measures the degree of aggregation or 'clumpiness' of a map based on the adjacency of patches of different classes |
| Shannon's diversity index | SDI | Quantifies the diversity of species in a given community |

**Table S2**. The table outlines the mathematical equations, units, value ranges, and references for various landscape metrics used in the analysis. The table provides the formulae and interpretations for these spatial pattern and fragmentation measures.

| Landscape Metrics | **Unit** | **Equation** | | **Range** | **References** |
|---|---|---|---|---|---|
| PD | Number per 100 ha | $\frac{NP}{TA}$ (ha$^{-1}$) | (**PD**): the number of patches of a certain type per unit area total landscape area (**A**) | 0≤PD≤maximum number of patches | (McGarigal & Marks 1995) |
| ED | (m/ha) | ED=$\frac{TE}{TCA}$ | (**TE**): the total landscape area (A) (**TCA**): constant, usually 10,000 or 100, that converts the units of ED to meters per hectare or kilometers per square kilometer | ED>0 | (McGarigal & Marks 1995) |
| LPI | Percent | LPI=$(1+x)^n = \frac{j=1\max(a)}{\sqrt{A}}(100)$ | (**a**): the area of the largest patch of a class (**A**): the total landscape area | 0≤LPI≤1 | (Saura S 2001) |
| A.I. | Percent | $\frac{e_{i.i}}{max - e_{i.i}}$ | (**e$_{i,i}$**): the number of like adjacencies involving the corresponding patch type (**max**): the maximum possible number of like adjacencies | -1≤A.I.≤1 | (Bogaert 2001) |
| PLAND | Percent | $\frac{a_i}{A} \times (100)$ | (**a$_i$**): total area of the patch type (**A**): the total landscape area | 0≤PLAND≤1 | (McGarigal & Marks 1995) |
| NP | None | NP = $n_i$ | (**n$_i$**): the number of patches of a class | NP ∈N | (Turner et al., 1989) |
| TE | Meters | $\sum_{1}^{NP} e\ (km)$ | (**e**): the edge length of a patch | TE>0 | (McGarigal et al., 1995) |
| LSI | None | $\frac{0.25\sum_{k=1}^{m}\theta}{\sqrt{A}}$ | (**A**): the total landscape area (**θ**): the perimeter of a patch | 0≤LSI≤higher values for more complex shapes | (Wu et al., 2016) |
| Split | None | $\frac{A_t^2}{\sum_{n=1}^{n} A_i^2}$ | (**A$_t$**): the total area of a class (**A$_i$**): the area of a patch of a class | Split>0 | (Jaeger et al., 2000) |
| IJI | Percent | $\frac{-\sum_{i=1}^{m}\ \sum_{k=i+1}^{m}\ \left[\left(\frac{e_{ik}}{E}\right) * \ln\left(\frac{e_{ik}}{E}\right)\right]}{\ln(0.5[m(m-1)])}(100)$ | (**e$_{ik}$**): the number of adjacencies between patch types i and k (**E**): is the total number of adjacencies. (**m**): is the total number of land use or land cover categories | -1≤IJI≤1 | (Bianchin et al., 2011) |
| SDI | Dimensionless | $H' = -\sum_{i=1}^{n} p_i\ lnp_i$ | (**H'**): Shannon Diversity Index (**n**) is the number of elements in the system, (pi) is the proportion of the i-th element | 0 ~ ln (s) | (McGarigal et al., 2012) |